NeuroImage 162 (2017) 65–72

Contents lists available at ScienceDirect

NeuroImage

journal homepage: www.elsevier.com/locate/neuroimage

Investigating the maturation of microstructure and radial orientation in the preterm human cortex with diffusion MRI

Zach Eaton-Rosen [a,*], Benoit Scherrer [b], Andrew Melbourne [a], Sebastien Ourselin [a], Jeffrey J. Neil [c], Simon K. Warfield [b]

[a] Translational Imaging Group, CMIC, UCL, UK
[b] Department of Radiology, Boston Childrens Hospital and Harvard Medical School, 300 Longwood Avenue, Boston, MA, USA
[c] Department of Neurology, Boston Children's Hospital, 333 Longwood Ave, LO450, 02115, Boston, MA, USA

A B S T R A C T

Preterm birth disrupts and alters the complex developmental processes in the cerebral cortex. This disruption may be a contributing factor to widespread delay and cognitive difficulties in the preterm population. Diffusion-weighted magnetic resonance imaging (DW MRI) is a noninvasive imaging technique that makes inferences about cellular structures, at scales smaller than the imaging resolution. One established finding is that DW MRI shows a transient radial alignment in the preterm cortex. In this study, we quantify this maturational process with the "radiality index", a parameter that measures directional coherence, which we expect to change rapidly in the perinatal period. To measure this index, we used structural T^2-weighted MRI to segment the cortex and generate cortical meshes. We obtained normal vectors for each face of the mesh and compared them to the principal diffusion direction, calculated by both the DTI and DIAMOND models, to generate the radiality index. The subjects included in this study were 89 infants born at fewer than 34 weeks completed gestation, each imaged at up to four timepoints between 27 and 42 weeks gestational age. In this manuscript, we quantify the longitudinal trajectory of radiality, fractional anisotropy and mean diffusivity from the DTI and DIAMOND models. For the radiality index and fractional anisotropy, the DIAMOND model offers improved sensitivity over the DTI model. The radiality index has a consistent progression across time, with the rate of change depending on the cortical lobe. The occipital lobe changes most rapidly, and the frontal and temporal least: this is commensurate with known developmental anatomy. Analysing the radiality index offers information complementary to other diffusion parameters.

1. Introduction

While infants survive preterm birth at increasing rates, it remains the primary cause of neonatal mortality, and associated morbidity often persists throughout the individual's lifetime. Preterm infants are more likely to suffer from cerebral palsy, cognitive deficits, loss of neuro-motor function and have long-term difficulties in education (Saigal and Doyle, 2008). These disabilities are among the highest-priority public health concerns in Europe and the U.S.A (Behrman and Butler, 2007), and are associated with extended costs for perinatal care and ongoing support into adulthood (Petrou, 2003). Research into this population is necessary to better describe and understand abnormal brain development in preterm infants. This will facilitate more accurate assessment of the likelihood of specific deficits, and enable improved comparison of strategies for early therapeutic intervention.

Diffusion-Weighted MRI (DW MRI) is a non-ionising, non-invasive imaging technique. It operates by sensitising the MRI signal to the bulk motion of molecular water, in several gradient directions and at varying diffusion length-scales. Because the diffusion of water is influenced by the local cellular structure, diffusion MRI characterises how water preferentially diffuses within an imaging voxel and is sensitive to cytoarchitecture on the scale of microns (Le Bihan, 2003). To compare and summarise diffusion properties across different acquisitions, subjects and in different voxels, a variety of mathematical models have been developed. One early model was diffusion tensor imaging (DTI) (Basser, 1995), which characterises the average diffusion in each voxel with a single, symmetric and positive-definite tensor. This model permits assessment of the average principal diffusion orientation and of the diffusion anisotropy, which is typically parameterised by the "fractional anisotropy" (FA).

For preterm infants, birth occurs during a critical time in neurodevelopment. This disruption has wide-ranging effects, with preterm infants showing reduced development of the cerebral cortex by term equivalent age (Ajayi-Obe et al., 2000). During early development, cortical neurons migrate radially outwards, on glial cells, towards the pial surface. This populates the cortex (Bystron et al., 2008) and causes a highly directional, coherent, columnar microstructural environment, which can be seen with DTI as tensors with high FA, oriented radially to

* Corresponding author.
E-mail address: z.eaton-rosen@ucl.ac.uk (Z. Eaton-Rosen).

http://dx.doi.org/10.1016/j.neuroimage.2017.08.013
Received 31 March 2017; Received in revised form 24 July 2017; Accepted 3 August 2017
Available online 8 August 2017

the cortical surface (McKinstry et al., 2002). In subsequent growth within the cortex, cross-connections develop, as dendrites and axons elaborate and obscure the underlying radial structure. In DW MRI, this manifests as a longitudinal reduction in FA (McKinstry et al., 2002), and less-aligned diffusion tensors. Following approximately 25 weeks gestation, a large majority of cortical folding and growth of cortical connections occurs. The cortex produces gyri and sulci, which occurs mostly postnatally for preterm infants. While the folding does not, in itself, change the microstructure, there are effects on DW MRI measurements, with microstructural maturation correlating with local cortical growth (Ball et al., 2013). Gyrification of the cortex will cause more partial volume effects between the cortical grey matter, and either the underlying white matter or the outlying cerebrospinal fluid (CSF). CSF in particular has different diffusion properties to tissue, and so removing the confound of CSF partial volume is important.

In recent times, technological aspects of DW MRI have advanced significantly. There is increasing sensitivity to diffusion (characterised by the *b*-value), more directions in a scan, and improved resolution. These improvements have spurred recent interest in diffusion within the cortex — both in terms of the DTI parameter values, and the directionality of water diffusion. DW MRI can now detect that the average direction of cortical diffusion is radial, even in adults (McNab et al., 2013). This study defined the "Radiality Index", which measures how orthogonal to the cortical surface the principal diffusion direction is. The orthogonal direction is called the "surface normal", and the radiality index is defined mathematically as the magnitude of the inner product of the principal direction of diffusivity with this surface normal vector. This radiality index was shown to correspond with known histology, and was shown to be greater than the value that would be expected by randomly-aligned tensors (0.5) in all except small regions of the cortex. In addition, Truong et al. (2014) have shown that the DTI parameters and the radiality index have a dependence on cortical depth that is detectable *in vivo*. In infants, it has been shown using the ball-and-stick model that radiality after preterm birth is higher (≥ 0.5) towards the anterior cortex, while it is ~ 0.5 in other regions (Melbourne et al., 2012).

In addition to improvements in the DW MRI acquisition, there have been advances in modelling the diffusion signal. With more diffusion data, it is possible to fit multiple compartments within a single voxel, so that the signal is a linear combination of the diffusion signals from structurally different environments. For example, the signal within white matter adjacent to the CSF could be modelled as combining an anisotropic tissue compartment with an isotropic tensor (ball) of fixed diffusivity (Behrens et al., 2003). The "DIstribution of 3D Anisotropic MicrOstructural eNvironments in Diffusion-compartment imaging" (DIAMOND) model (Scherrer et al., 2016) is an example of this approach. DIAMOND enables the assessment of the relative signal fraction of each compartment, as well as compartment-specific characteristics such as the compartment fractional anisotropy (cFA), and the compartment mean diffusivity (cMD).

While some advanced diffusion models have been used in the preterm population (Kunz et al., 2014; Eaton-Rosen et al., 2015), this richer characterisation of the microstructure has not yet been fully explored. In this manuscript, we quantify the trajectories of development for cortical radiality as a function of the cortical region. By using structural and diffusion-weighted MRI in tandem, we present the first longitudinal assessment of the radiality index in preterm infants. DIAMOND offers an explicit modelling of partial volume to deal with small brains and changing cortical convolution, while the tensor component in the model can be used to assess the principal direction without the confound of CSF. Measuring the deviation in growth patterns may be of use in clinical prognosis.

In this work, we quantify the longitudinal changes in radial diffusion within the preterm cortex for the first time *in-vivo*. These measurements are of interest as an insight into general neurodevelopment, as well as further elucidating our knowledge of possible effects of prematurity.

2. Methods

2.1. MRI acquisition and participation

We recruited infants born at fewer than 34 weeks completed gestation from the St Louis Childrens Hospital Neonatal Intensive Care Unit (NICU) between 2007 and 2010. These infants were scanned at up to four different age intervals postnatally: < 30, 30–31, 34–35, and 38–40 weeks gestational age. The average gestational age at birth was 26.9 ± 2.1 weeks, with the range being 23–33 weeks. Due to health complications and challenges inherent in scanning infants, not all of the scans were performed — of 105 surviving infants with no intra-ventricular haemorrhage, 89 subjects had useable MRI data from one more more scanning sessions. Of these, 37 had data from a single point in time; a further 37 were scanned at two timepoints, 12 had three timepoints and 3 were scanned at all four timepoints. Images were acquired when infants were resting or asleep, after feeding, wrapping and delivery to the MRI machine as outlined in (Mathur et al., 2008). Studies were approved by the Washington University Human Studies Committee.

The MRI was acquired with a 3-T Siemens TIM Trio system (Erlangen, Germany) using an infant-specific, quadrature head coil (Advanced Imaging Research, Cleveland, OH, USA). The structural scans were a T_2-weighted fast spin echo sequence (repetition time (T_R) 8500 ms, echo time (T_E) 160 ms, $1\times1\times1$ mm^3 voxels) and a rapid gradient echo T_1-weighted acquisition with resolution of $1\times1\times1$ mm^3 voxels (T_R/T_E:1 500/3 ms).

The diffusion acquisition consisted of 48 gradient directions with *b*-values ranging to cover values from 0 to 1 200 s/mm^2. The acquisition parameters were: T_R 13,300 ms, T_E 112 ms, 1 266 Hz/Px bandwidth, 128 mm field of view (FoV), $1.2 \times 1.2 \times 1.2$ mm^3 voxels. Total acquisition was approximately 60 min in duration. The *b*-values were: 0, 0, 0, 75, 80, 85, 150, 160, 171, 225, 240, 257, 300, 320, 342, 375, 400, 428, 450, 480, 514, 525, 560, 600, 600, 640, 675, 685, 720, 750, 771, 800, 825, 857, 880, 900, 942, 960, 975, 1028, 1040, 1050, 1114, 1120, 1125, 1200, 1200, and 1200 mm^2 s^{-1}. We inspected each acquired volume and discarded those with significant motion artifacts from movement during the acquisition, removing an average of 3.0±3.5 volumes per infant. We co-registered the scans affinely to an average $b = 0$ image in order to eddy-correct and to correct for motion between acquisitions.

The data processing pipeline is illustrated in Fig. 1, with each step being detailed below.

2.2. Image segmentation

As intermediate steps in this investigation, we produced a surface mesh of the cortex and labelled the cortical lobes for each subject. The cortical mesh was computed from a probabilistic segmentation of the cortical grey matter. For this, we initialised a preterm-specific segmentation algorithm (Cardoso et al., 2013) with a probabilistic atlas of the developing brain (Kuklisova-Murgasova et al., 2011). This was performed on T_2-weighted data, because of the high contrast between cortex and white matter, and produced a segmentation of the brain into white matter, cortical grey matter and CSF. We further segmented the brain into the occipital, parietal, frontal and temporal lobes using Geodesic Information Flows (GIF) (Cardoso et al., 2015), using a newborn atlas (Gousias et al., 2012). We combined the tissue segmentation with the maps of the lobes to produce cortical segmentations with a lobe label, to investigate diffusion parameters on a regional basis.

2.3. The DIAMOND model

The outlying cerebrospinal fluid has a large impact on diffusion readings in the cortex. To explicitly model this partial volume, we could have employed the ball-and-stick model (Behrens et al., 2007) to assess the diffusion orientation in each voxel. However it does not provide diffusion characteristics of the tissue compartment, because the stick

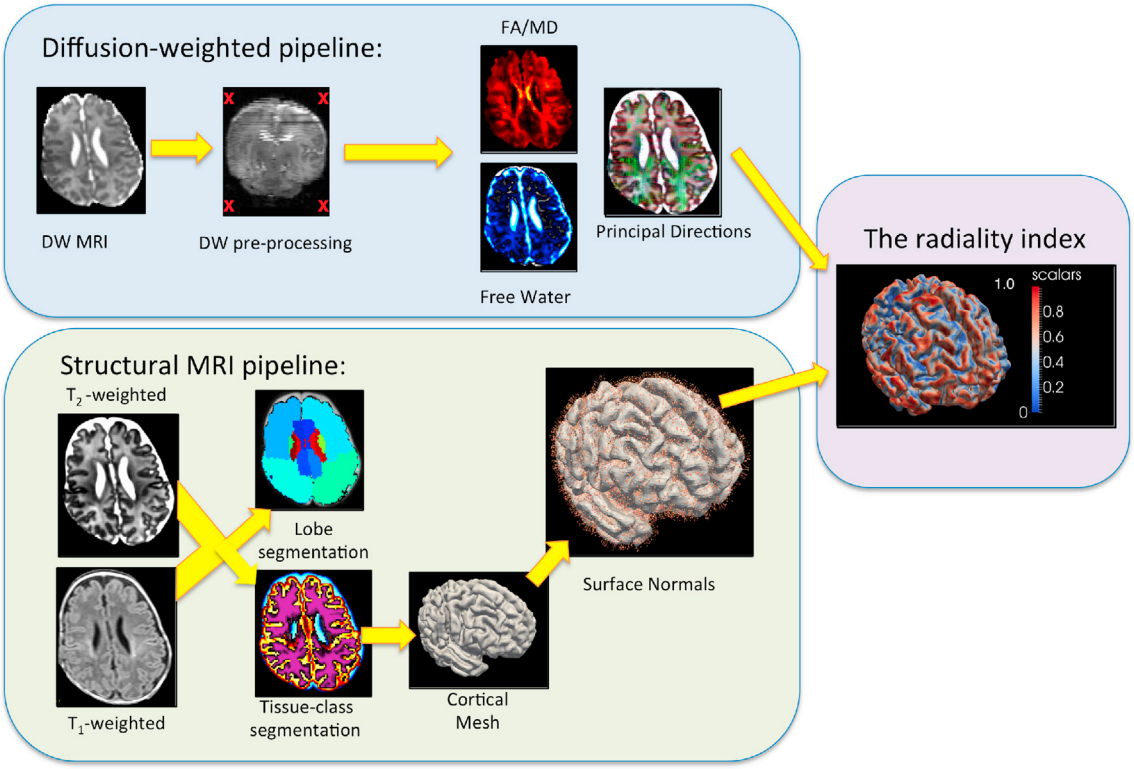

Fig. 1. The data-processing pipeline. Within-subject, within-timepoint, data was aligned into the space of theT_2-weighted image. The tissue-class segmentation used priors from an age-specific atlas to initialise an expectation-maximisation segmentation on the structural image. This segmentation was split into hemispheres, and we extract the largest connected component of the white matter and cortex segmentations, to ensure that the topology was correct. We then used CRUISE to generate a cortical surface. The normal vectors were calculated from the triangular faces, a random subset of which is shown in the 'surface normals' above. The diffusion data was processed using DIAMOND to generate free-water maps and a tensor map for the tissue component, and also with DTI.

parameters are fixed and identical throughout the brain. By contrast, DIAMOND provides both:

1. The diffusion principal orientation to calculate the radiality index, and
2. The compartment-specific parameters (cFA, cMD) similar to those of DTI, to evaluate microstructure properties.

We used the DIAMOND model (Scherrer et al., 2016) with two compartments: an isotropic diffusion compartment with fixed diffusivity to model CSF contamination, and an anisotropic tissue compartment to model diffusion within the tissue. DIAMOND models the anisotropic diffusion compartment with a statistical distribution of diffusion tensors to account for the heterogeneity of the underlying microstructure. Assessing the average tensor of the distribution allows characterisation of the average diffusion characteristics in the compartment, from which compartment-specific parameters (compartment FA and compartment MD, denoted cFA and cMD respectively) can be inferred. Moreover,

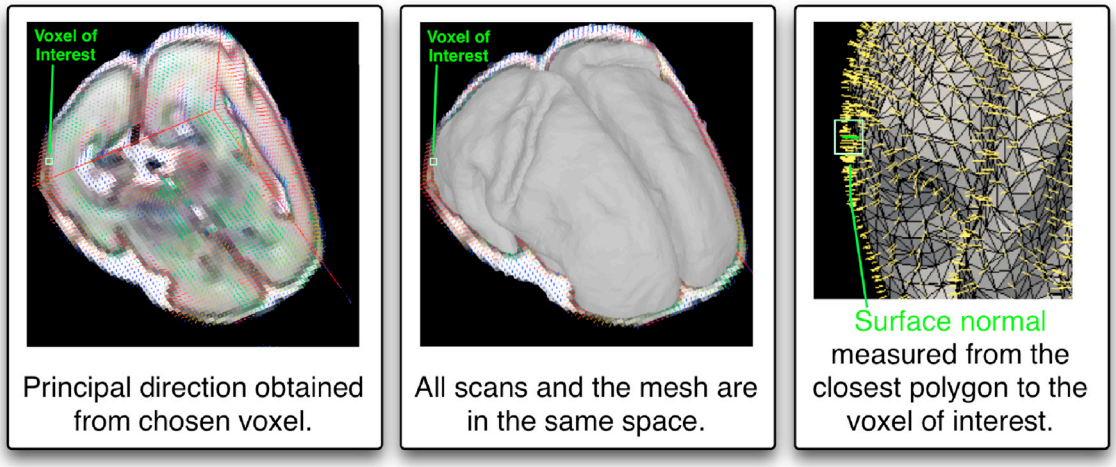

Fig. 2. This figure demonstrates the process for acquiring the principal diffusion direction **v** and surface normal **r** for a given voxel. For a given voxel of interest, we first determine **v** by fitting the desired diffusion model (leftmost panel — note that this view is displaying information on 3 axes, not one slice). We then identify the closest triangular mesh face to this point, using the surface mesh. By taking the cross-product of any two edges of this triangular face, we obtain **r**. In calculating $|\mathbf{r}.\mathbf{v}|$, it is not important to ensure that **r** faces outwards, because the diffusion acquisition only tells us about water diffusion along a line segment, not in a particular direction.

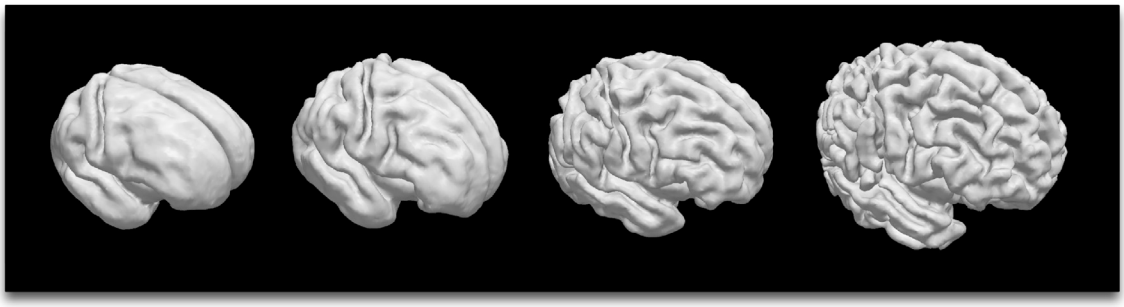

Fig. 3. This figure displays the cortical mesh at four timepoints for the same infant. The infant was born at 28 weeks estimated gestational age (GA), and these scans are, from left-right, at 28, 30, 33 and 38 weeks GA respectively. The cortex has progressed from broadly flat to highly convoluted during the ten postnatal weeks between images.

DIAMOND provides an index describing the intra-compartment heterogeneity, based on the concentration of the distribution of tensors. Other multi-compartment models often require higher b-values (for example, NODDI (Zhang et al., 2012) recommends including *b*-values of 2000mm^{2}s^{-1} for infants), and so were unsuitable to our data.

2.4. Calculating the radiality index

The radiality in a given voxel was determined from two separate measurements. One is the principal diffusion direction, which we compute using both DTI and DIAMOND. This results in a radiality index for each model, to compare DIAMOND and DTI for this application. The other is to calculate vectors that are locally normal to the cortical surface (pointing outwards). A high radiality index arises when this surface normal is approximately collinear with the principal diffusion direction, and lower when the directions diverge.

To calculate the cortical mesh of the cortical surface, we used implicit surface evolution (CRUISE) (Han et al., 2004) on the tissue segmentations, and topology-corrected the mesh with a fast-marching algorithm (Bazin and Pham, 2007). The surface mesh inherently defines a normal vector at each triangular face (the direction is given by taking the cross-product of any two edges of each triangle).

For each voxel in the diffusion parameter maps, the radiality index is given as:

$$\frac{|\mathbf{r}.\mathbf{v}|}{||\mathbf{r}||||\mathbf{v}||} \quad (1)$$

This is the magnitude of the dot product of the radial vector nearest the voxel **r** with the principal eigenvector of the diffusion tensor, **v**, normalised by the vector lengths. This process is illustrated in Fig. 2.

The small size of the infant brain, relative to the scanning resolution, introduces challenges in computing a surface normal for each voxel in the cortex. We were aiming to measure the changes within the cortical tissue caused by maturation, without the confound of morphological change. To compute the radiality within a voxel, we must ensure that the tissue is homogeneous (i.e. no partial volume with another, folded, part of the cortex) and that the surface normal is coherent at that point (i.e. the surface is relatively flat within the voxel). To eliminate the partial volume with cortical tissue, we excluded regions in the sulci. The sulci not only have more partial volume, but are also more curved than the gyri, so excluding these provided more coherent orientations of the normals. To perform this masking, we computed the mean curvature over the cortical surface, and analysed regions only where the surface was convex (mean curvature <0). This means that we ignored the radiality in the sulci, in favour of having a flatter surface and more reliable radial vectors.

2.5. Statistical approach

For data analysis, it was necessary to account for missing data, the unbalanced sampling of time-points, and correlations in data from the subjects who are scanned longitudinally. To do this, we used models with fixed and random effects — known as mixed models. This type of modelling has been used to build normative curves for neurodevelopment, using DTI (Sadeghi et al., 2013, 2014). Fixed effects quantify the population-level effects, while random effects allow the model parameters to vary on a per-subject basis.

In order to analyse which effects were significant in the models, we used backwards elimination of non-significant effects of a linear mixed-effects model. For a given diffusion metric *y*, in a given cortical lobe, of subject i at time t, we fitted a model that included available subject information: the sex (S_i), gestational age at birth (GA_i), the estimated gestational age (t) and the hemisphere the measurement was taken in (H). The random effect is an intercept that varies on a per-subject basis (b_i) and ε is an error term.

$$y_i(t) = \alpha_0 + \alpha_1 S_i + \alpha_2 H + \alpha_3 GA_i + \beta t + b_i + \varepsilon \quad (2)$$

To compensate for multiple comparisons with the 6 diffusion

Table 1
This table shows the coefficients for the models of the diffusion parameters. Note that for each of the diffusion parameters, the preferred model took the form of $y_i(t) = \alpha_0 + \beta t + b_i + \varepsilon$, and thus effects from hemisphere, GA at birth, and sex were not found to contribute significantly to the model fit. In this table we display the intercept at 27 weeks (α_0) and the slope β.

	Intercept±SE (at 27 weeks)	Slope±SE (per week)	Intercept±SE (27 weeks)	Slope±SE (per week)
	cFA		FA	
Frontal Lobe	0.175 ± 0.003	-0.0089 ± 0.0003	0.168 ± 0.002	-0.0033 ± 0.0002
Occipital Lobe	0.159 ± 0.004	-0.0089 ± 0.0004	0.194 ± 0.004	-0.0058 ± 0.0004
Parietal Lobe	0.177 ± 0.003	-0.0094 ± 0.0003	0.180 ± 0.002	-0.0053 ± 0.0002
Temporal Lobe	0.191 ± 0.003	-0.0107 ± 0.0003	0.187 ± 0.003	-0.0049 ± 0.0004
	cMD/10^{-3}mm^{2}s^{-1}		MD/10^{-3}mm^{2}s^{-1}	
Frontal Lobe	1.13 ± 0.008	-0.0024 ± 0.0009	1.37 ± 0.009	-0.0098 ± 0.0009
Occipital Lobe	1.12 ± 0.011	-0.0032 ± 0.0010	1.41 ± 0.013	-0.0111 ± 0.0014
Parietal Lobe	1.18 ± 0.008	-0.0054 ± 0.0008	1.38 ± 0.008	-0.0140 ± 0.0008
Temporal Lobe	1.10 ± 0.009	-0.0029 ± 0.0010	1.40 ± 0.009	-0.0124 ± 0.0001
	DIAMOND Radiality		DTI Radiality	
Frontal Lobe	0.961 ± 0.008	-0.0189 ± 0.0008	0.898 ± 0.008	-0.0126 ± 0.0009
Occipital Lobe	0.952 ± 0.009	-0.0323 ± 0.0008	0.859 ± 0.009	-0.0206 ± 0.0009
Parietal Lobe	0.945 ± 0.008	-0.0227 ± 0.0008	0.891 ± 0.008	-0.0158 ± 0.0008
Temporal Lobe	0.901 ± 0.008	-0.0190 ± 0.0009	0.844 ± 0.008	-0.0124 ± 0.0008

parameters we analysed ({DTI/DIAMOND} × {FA/MD/Radiality}), we fixed the threshold for including fixed effects at 0.05/6 (Bonferroni correction). We performed all data analysis in R (v3.2.1), using the package "lmer" (v1.1.12) (Bates et al., 2015). We used "lmerTest" [Kuznetsova et al.] for performing the backwards elimination.

3. Results

The automatic segmentation and subsequent mesh generation produced cortical meshes for all timepoints in the study. For an example of typical longitudinal progression in this study, see Fig. 3.

For all of the regions and diffusion parameters tested, the elimination of non-significant effects removed the effects of sex, hemisphere and gestational age at birth. Thus, for each parameter and in each region, the preferred model was a linear model that depended on time. The parameters for the model are shown in Table 1.

Fig. 4 shows that fractional anisotropy decreased for both the DIAMOND and DTI models. The slopes were greater in magnitude (see Table 1) for the DIAMOND model ($p < 10^{-7}$ for all regions, using a *t*-test) than the DTI model.

For mean diffusivity, the DTI model had a significantly greater intercept than the DIAMOND model's cMD ($p < 10^{-9}$) for all regions). The slope was of greater magnitude for the DTI model ($p < 10^{-9}$) for all regions). See Fig. 4, and Table 1.

In Fig. 5 we present the cortical radiality for the DTI and DIAMOND models during the preterm period. The frontal and temporal lobes decrease at statistically indistinguishable rates from each other ($p = \{0.93|0.86\}$ for {DIAMOND|DTI} respectively), but significantly lower rates than the parietal lobe and the occipital lobe ($p < 10^{-4}$). The occipital lobe decreased with the largest rate for both DIAMOND and DTI ($p < 10^{-4}$). The DIAMOND model had a greater rate of decrease than the DTI model in all regions ($p < 10^{-8}$), which is consistent with DIAMOND reducing the impact of CSF contamination. The intercepts were higher in DIAMOND ($p < 10^{-7}$) than for DTI.

4. Discussion

Because cortical folding and neuronal elaboration are broadly complete for infants delivered at term, preterm MRI offers a unique chance to image these maturational processes *ex-utero*. The rapid changes in the cortex during the perinatal period are critical events in neurodevelopment. In this work, we have evaluated the radiality index and diffusion tensor parameters in preterm infants on a longitudinal basis. We have shown a decrease in cortical radiality, cFA and FA in each lobe of the cortex, with region-specific rates. None of the models showed any sex-dependence, in agreement with (Young et al., 2016).

In terms of diffusion tensor parameters, both DTI and DIAMOND showed expected reductions in (c)FA, which is theorised to relate to elaboration of the microstructural environment and consequent reduction in anisotropy (McKinstry et al., 2002). The MD decreased significantly more in the DTI model than for the cMD, which could be attributed to the DIAMOND model having an explicit model of CSF partial volume. This feature allows the DIAMOND model to remove the confound of CSF partial volume in the cortex, and examine only the tissue.

The radiality index is close to unity at early timepoints in the study for both DIAMOND and DTI, reflecting the highly-ordered and radial nature of the supporting glial cells. As the cortex matures, overlying fibres are added to this radial substrate. We suggest that the reduction in measured radiality reflects, at least in part, this microstructural change. At early timepoints, the extra-cellular water is hindered orthogonal to the fibres,

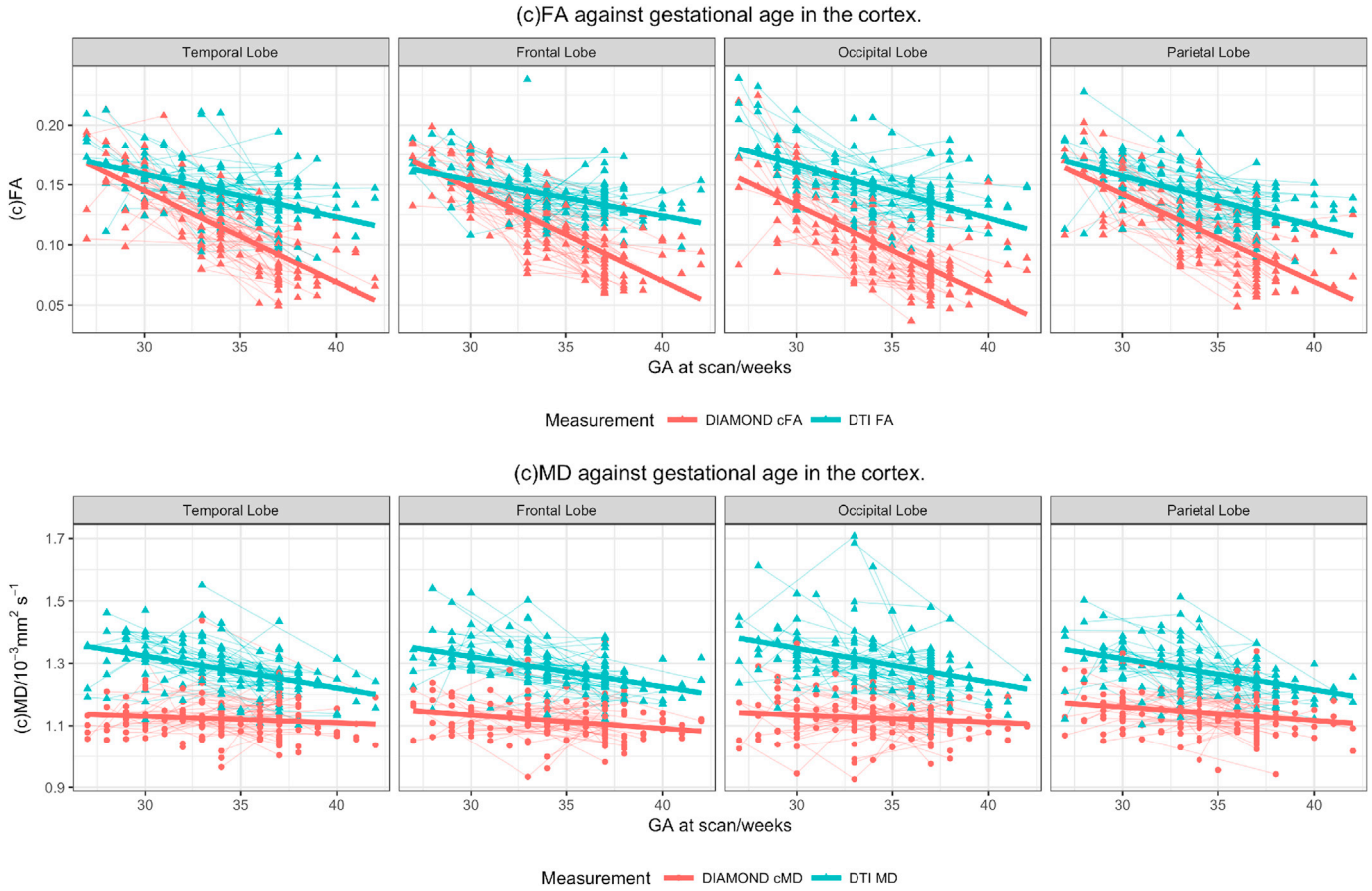

Fig. 4. The mean values for (c)FA and (c)MD in the DIAMOND and DTI models. Dashed lines connect longitudinal measurements from the same infant. The trend lines are the population trends from the linear models in Table 1, which were modelled by extracting the coefficients from the model fits, and predicting with random effects set to 0.

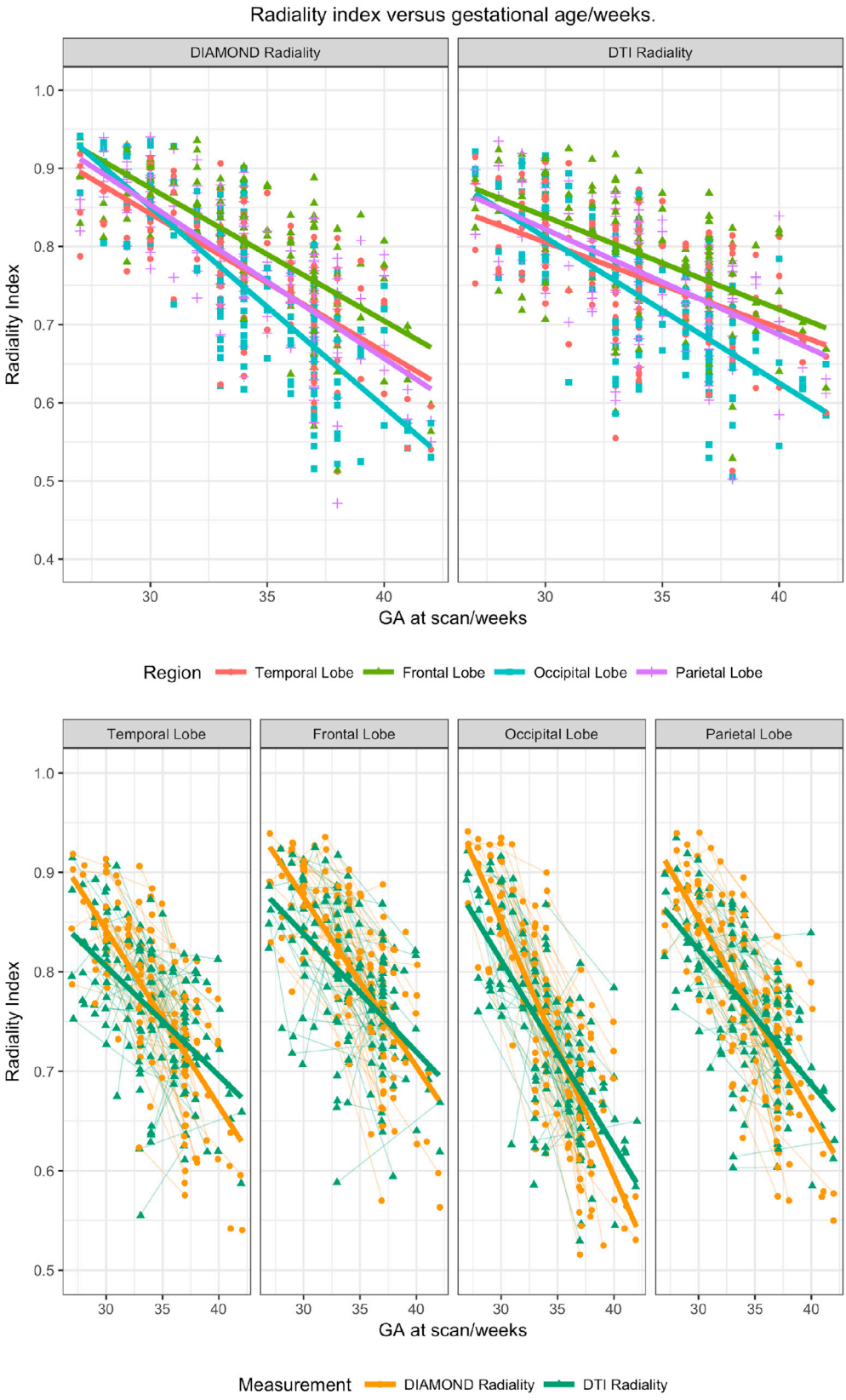

Fig. 5. The mean values for the radiality index for DIAMOND and DTI models in each lobe. Bold lines are linear trendlines, with parameters from Table 1. DTI and the DIAMOND model show similar trends in radiality (top figure), with the rate of change being greatest for the occipital lobe. The DIAMOND model shows significantly greater changes than the DTI model over the time period for each region.

and thus has a principal direction of diffusivity that augments the radial structure of the intra-cellular compartment. This extra-cellular space reduces significantly in development, which contributes to the measured decline in radiality. We found that the rate of change of radiality depends on the lobe, with the occipital lobe having the highest rate of change. None of the MD, cMD, FA or cFA had the greatest rates of change in the occipital lobe, which is evidence that the radiality index is not solely reflecting these known parameters, and thus that this parameter provides complementary information to traditional diffusion measures.

In (der Knaap et al., 1996), the authors graded the "gyral development score" as a function of GA. They found that the medial occipital area develops fastest, while the frontal lobe (minus the area of the central sulcus) and anterior part of the temporal lobe develop slowest. The parietal lobe, the posterior part of the temporal lobe, and the occipital lobe (minus the medial area) were in between. This fits with our finding with the radiality index: that the occipital lobe develops the most rapidly, and the frontal and temporal lobes have the smallest rate of change. This also suggests that breaking down the cortex into smaller regions of interest would also be of interest. The fact that our measured rates correlated with trends in gyrification is also in agreement with the finding that microstructural maturation is concurrent with local macrostructural growth (Ball et al., 2013).

4.1. Comparing DIAMOND and DTI

Comparing the values for the DIAMOND and DTI radialities, we observed that the DIAMOND model measured higher radialities at early timepoints, and lower at later timepoints than DTI. This could, perhaps, be attributed to an increased sensitivity to the structure by using the multi-compartment formalisation of DIAMOND. Being able to explicitly model the partial volume is important within the rapidly-folding cortex.

The cFA reached a lower value than the FA by term-equivalent age, which was not expected. It is likely that the DIAMOND model is more able to account for measurement noise than the tensor formulation, which is an advantage in the low SNR regime of the infant cortex. This could be because of the spatial regularisation in the fitting of the DIAMOND model, which acts to reduce spuriously high FA values caused by noise.

For the fractional anisotropy and radiality, DIAMOND displayed significantly higher changes in parameter values than the DTI model. However, the changes in cMD were significantly lower in magnitude than in the DTI model. This is likely to be because of less partial volume with CSF, so some fraction of the observed MD change is likely to be spurious.

4.2. Limitations

The radiality calculated at each voxel depends on many factors, including the accuracy of the cortical mesh, the quality of alignment between modalities, and the diffusion-weighted data at a given voxel. The radiality is bounded between 0 and 1, with values expected to be near to 1 in much of the brain (entirely radial diffusion). Thus, errors are, especially at early time-points, expected to *underestimate* the radiality, causing the bias in the error to be time-dependent.

Despite the concurrence in radiality change with development, relating the parameter directly to the microstructure is challenging. While the intuitive picture is of radiality decreasing as cells are added to the cortex, we know that these fibres are being added to a persistent radial substrate. Because this direction persists, we may have expected that the radiality would be constant throughout development. Some element of the reduction in radiality may be because the restrictions lead to more attenuation in all directions, and hence a noisier signal, which may perturb the principal direction of the diffusion model. However, it is highly implausible that this confound would cause the major finding of the large reduction in cortical radiality from 27 to 42 weeks gestational age.

Several scans had some evidence of motion artifacts. While all data was individually inspected for quality, different infants had different numbers of diffusion volumes. Similarly, there are some cortical meshes with unphysical folds or ridges introduced by the algorithm. However, any automatic procedure will have some errors against the gold-standard of manual segmentation, but manual segmentation would have been impractical and time-consuming for this number of scans. While these issues affect the presented work, this does not detract from our overall findings of large reductions in cortical radiality during development.

In terms of statistical approach, other work in this domain has used *non*-linear mixed effects models, often with parameters that have biophysical interpretations (Sadeghi et al., 2013, 2014). These nonlinear models require a much greater longitudinal range that that available to us, and thus, a linear model is appropriate, and can be seen as a local approximation to a non-linear curve. While adult radiality values could be used as a fixed asymptote, this would make too many assumptions about both the parameter values throughout childhood, and the comparability of this method to published work on adults, which uses different acquisitions and processing pipelines.

4.3. Future work

We could extend our work in measuring radiality in large regions of the cortex to smaller regions of interest, such as in (McNab et al., 2013; Deipolyi et al., 2005). We did not, partly because automatic segmentation tools for cortical analysis of infants lag their adult counterparts, owing in part to the peculiar difficulties, so the labels are not available. It would also have the downside of reducing the statistical power available to compare the regions by reducing the number of voxels in each.

While the current work characterises a cohort of preterm-born infants, more investigation would be required to use an individual's radiality scores as a basis for prognosis. Future work could go further in defining normal values for this index, and correlating scores with clinical outcome.

Although our DW acquisition had a high resolution, the *b*-value was limited to $\leq 1200\text{mm}^2\text{s}^{-1}$. Higher *b*-values may warrant using a more sophisticated model of diffusion within the cortex. An intuitive model would be a directional component oriented radially, that is augmented by an oblate disk orthogonal to this axis, representing the new fibres. This type of model would separate contributions to the radiality as coming from radial fibres or perpendicular additions. Our model has, however, the advantage of being comparable to other radiality studies.

5. Conclusions

In this manuscript, we have produced the first analysis of the change in cortical radiality in preterm neonates, as imaged by DW MRI. During the preterm period, the geometry of water diffusion matures rapidly from its almost entirely radial state at 27 weeks gestational age. The radiality index shows promise as an early marker of cortical development, and offers a quantification of the observed decrease in directional coherence. The DIAMOND model offers increased sensitivity to these changes when compared to the DTI model.

Conflicts of interest

None declared.

Acknowledgements

This work was supported in part by the EPSRC-funded UCL Centre for Doctoral Training in Medical Imaging (EP/L016478/1), BRC/90/HI/SO and MR/J01107X/1. This work was also supported by the National Institutes of Health (grant numbers R01 HD05709801, R01 EB019483, R01 NS079788, R01 EB013248, R01 EB018988, R42 MH086984, and U01 NS082320). The funders had no role in study design, data collection, and analysis, decision to publish or preparation of the manuscript.

We acknowledge the members of the research team who assisted in acquiring the MRI scans and performing data analysis, including Joseph Ackerman, Karen Lukas, Anthony Barton, Michael Wallendorf, Erin Reynolds, and Kayla Hannon.

We also acknowledge the help of Dr. Eliza Orasanu for her advice on generating the cortical meshes, and Dr Brian Monson for stimulating discussion. Finally, we thank the many infants and families who participated in the investigation for their generous assistance and dedication.

References

Ajayi-Obe, M., Saeed, N., Cowan, F.M., Rutherford, M.A., Edwards, A.D., 2000. Reduced development of cerebral cortex in extremely preterm infants. Lancet 356 (9236), 1162–1163.

Ball, G., Srinivasan, L., Aljabar, P., Counsell, S.J., Durighel, G., Hajnal, J.V., Rutherford, M.A., Edwards, A.D., 2013. Development of cortical microstructure in the preterm human brain. Proc. Natl. Acad. Sci. U. S. A. 110 (23), 9541–9546.

Basser, P., 1995. Inferring microstructural features and the physiological state of tissues from diffusion-weighted images. NMR Biomed. 8, 334–344.

Bates, D., Mächler, M., Bolker, B., Walker, S., 2015. Fitting linear mixed-effects models using {lme4}. J. Stat. Softw. 67 (1), 1–48.

Bazin, P.-L., Pham, D.L., 2007. Topology correction of segmented medical images using a fast marching algorithm. Comput. Methods Programs Biomed. 88 (2), 182–190.

Behrens, T.E.J., Berg, H.J., Jbabdi, S., Rushworth, M.F.S., Woolrich, M.W., 2007. Probabilistic diffusion tractography with multiple fibre orientations: what can we gain? NeuroImage 34 (1), 144–155.

Behrens, T.E.J., Woolrich, M.W., Jenkinson, M., Johansen-Berg, H., Nunes, R.G., Clare, S., Matthews, P.M., Brady, J.M., Smith, S.M., 2003. Characterization and propagation of uncertainty in diffusion-weighted MR imaging. Magnetic Reson. Med. official J. Soc. Magnetic Reson. Med./Soc. Magnetic Reson. Med. 50 (5), 1077–1088.

Behrman, R., Butler, A., 2007. Preterm Birth: Causes, Consequences, and Prevention. Institute of Medicine (US) Committee on Understanding Premature Birth and Assuring Healthy Outcomes.

Bystron, I., Blakemore, C., Rakic, P., 2008. Development of the human cerebral cortex: boulder Committee revisited. Nat. Rev. Neurosci. 9 (2), 110–122.

Cardoso, M.J., Melbourne, A., Kendall, G.S., Modat, M., Robertson, N.J., Marlow, N., Ourselin, S., 2013. AdaPT: an adaptive preterm segmentation algorithm for neonatal brain MRI. NeuroImage 65, 97–108.

Cardoso, M.J., Modat, M., Wolz, R., Melbourne, A., Cash, D., Rueckert, D., Ourselin, S., 2015. Geodesic information Flows: spatially-variant graphs and their application to segmentation and fusion. IEEE Trans. Med. Imaging 34 (9), 1976–1988.

Deipolyi, A.R., Mukherjee, P., Gill, K., Henry, R.G., Partridge, S.C., Veeraraghavan, S., Jin, H., Lu, Y., Miller, S.P., Ferriero, D.M., Vigneron, D.B., Barkovich, A.J., 2005. Comparing microstructural and macrostructural development of the cerebral cortex in premature newborns: diffusion tensor imaging versus cortical gyration. NeuroImage 27 (3), 579–586.

der Knaap, M.S., van Wezel-Meijler, G., Barth, P.G., Barkhof, F., Adèr, H.J., Valk, J., 1996. Normal gyration and sulcation in preterm and term neonates: appearance on MR images. Radiology 200 (2), 389–396.

Eaton-Rosen, Z., Melbourne, A., Orasanu, E., Cardoso, M.J., Modat, M., Bainbridge, A., Kendall, G.S., Robertson, N.J., Marlow, N., Ourselin, S., 2015. Longitudinal measurement of the developing grey matter in preterm subjects using multi-modal MRI. NeuroImage 111, 580–589.

Gousias, I.S., Edwards, A.D., Rutherford, M.A., Counsell, S.J., Hajnal, J.V., Rueckert, D., Hammers, A., 2012. Magnetic resonance imaging of the newborn brain: manual segmentation of labelled atlases in term-born and preterm infants. NeuroImage 62 (3), 1499–1509.

Han, X., Pham, D.L., Tosun, D., Rettmann, M.E., Xu, C., Prince, J.L., 2004. CRUISE: cortical reconstruction using implicit surface evolution. NeuroImage 23 (3), 997–1012.

Kuklisova-Murgasova, M., Aljabar, P., Srinivasan, L., Counsell, S.J., Doria, V., Serag, A., Gousias, I.S., Boardman, J.P., Rutherford, M.A., Edwards, A.D., Hajnal, J.V., Rueckert, D., 2011. NeuroImage A dynamic 4D probabilistic atlas of the developing brain. NeuroImage 54 (4), 2750–2763.

Kunz, N., Zhang, H., Vasung, L., O'Brien, K., 2014. Assessing white matter microstructure of the newborn with multi-shell diffusion MRI and biophysical compartment models. NeuroImage 96, 288–299.

Kuznetsova A., Brockhoff P. B., and Christensen R. H. B. Package LmerTest'.

Le Bihan, D., 2003. Looking into the functional architecture of the brain with diffusion MRI. Nat. Rev. Neurosci. 4 (6), 469–480.

Mathur, A.M., Neil, J.J., McKinstry, R.C., Inder, T.E., 2008. Transport, monitoring, and successful brain MR imaging in unsedated neonates. Pediatr. Radiol. 38 (3), 260–264.

McKinstry, R.C., Mathur, A., Miller, J.H., Ozcan, A., Snyder, A.Z., Schefft, G.L., Almli, C.R., Shiran, S.I., Conturo, T.E., Neil, J.J., 2002. Radial organization of developing preterm human cerebral cortex revealed by non-invasive water diffusion anisotropy MRI. Cereb. cortex 12 (12), 1237–1243. New York, N.Y. : 1991.

McNab, J.A., Polimeni, J.R., Wang, R., Augustinack, J.C., Fujimoto, K., Stevens, A., Janssens, T., Farivar, R., Folkerth, R.D., Vanduffel, W., Wald, L.L., 2013. Surface based analysis of diffusion orientation for identifying architectonic domains in the in vivo human cortex. NeuroImage 69, 87–100.

Melbourne, A., Kendall, G.S., Cardoso, M.J., Gunney, R., Robertson, N.J., Marlow, N., Ourselin, S., 2012. Radial structure in the preterm cortex; persistence of the preterm phenotype at term equivalent age?. In: Medical Image Computing and Computer-assisted Intervention : MICCAI … International Conference on Medical Image Computing and Computer-assisted Intervention, vol. 15, pp. 256–263. Pt 3.

Petrou, S., 2003. Economic consequences of preterm birth and low birthweight. BJOG Int. J. Obstetrics Gynaecol. 110, 17–23. April.

Sadeghi, N., Fletcher, P.T., Prastawa, M., Gilmore, J.H., Gerig, G., 2014. Subject-specific prediction using nonlinear population modeling: application to early brain maturation from DTI. In: Lecture Notes in Computer Science (Including Subseries Lecture Notes in Artificial Intelligence and Lecture Notes in Bioinformatics), vol. 8675. LNCS, pp. 33–40.

Sadeghi, N., Prastawa, M., Fletcher, P.T., Wolff, J., Gilmore, J.H., Gerig, G., 2013. Regional characterization of longitudinal DT-MRI to study white matter maturation of the early developing brain. NeuroImage 68, 236–247.

Saigal, S., Doyle, L.W., 2008. An overview of mortality and sequelae of preterm birth from infancy to adulthood. Lancet 371 (9608), 261–269.

Scherrer, B., Schwartzman, A., Taquet, M., Sahin, M., Prabhu, S.P., Warfield, S.K., 2016. Characterizing brain tissue by assessment of the distribution of anisotropic microstructural environments in diffusion-compartment imaging (DIAMOND). Magnetic Reson. Med. 76 (3), 963–977.

Truong, T.K., Guidon, A., Song, A.W., 2014. Cortical depth dependence of the diffusion anisotropy in the human cortical gray matter in vivo. PLoS ONE 9 (3).

Young, J.M., Morgan, B.R., Whyte, H.E., Lee, W., Smith, M.L., Raybaud, C., Shroff, M.M., Sled, J.G., Taylor, M.J., 2016. Longitudinal study of white matter development and outcomes in children born very preterm. Cereb. Cortex 1–12.

Zhang, H., Schneider, T., Wheeler-Kingshott, C.A., Alexander, D.C., 2012. NODDI: practical in vivo neurite orientation dispersion and density imaging of the human brain. NeuroImage 61 (4), 1000–1016.